J. Phys. B: At. Mol. Opt. Phys. **46** (2013) 245005 (8pp) doi:10.1088/0953-4075/46/24/245005

Floquet calculations of ionization of the molecular hydrogen ion by intense laser fields in the low-frequency limit

Ts Tsogbayar and M Horbatsch

Department of Physics and Astronomy, York University, 4700 Keele Street, Toronto, Ontario M3J 1P3, Canada

E-mail: marko@yorku.ca

Received 7 August 2013, in final form 10 October 2013
Published 4 December 2013
Online at stacks.iop.org/JPhysB/46/245005

Abstract

The coupled-channel Floquet equations in both length and velocity gauges are solved in a pseudospectral representation to analyse ionization of the lowest two electronic states of the H_2^+ ion by strong continuous laser fields. A complex absorbing potential is used to obtain Siegert-type solutions resulting in accurate resonance positions and widths. The roles of two possible ionization mechanisms, tunnel ionization and resonance excitation multi-photon ionization are explored. The ionization rates of the lower and upper states, which correspond to gerade and ungerade states in the field-free case are investigated as a function of internuclear separation R. The previously investigated double-peak structure at $\omega = 0.0428$ au is studied systematically as ω is decreased towards zero to understand how it relates to a similar structure in the dc limit. It is shown that the connection is not straightforward, since the ionization rates for the two states do mix strongly as ω is reduced for both peak regions. The mixing becomes pronounced even for the first peak around $R = 5$ au when $\omega < 0.02$ au. For the outer peak around $R = 9.5$ au, we find that the rates for the upper and lower states become the same at $\omega = 0.01$ au and correspond to 10–15% of the upper-state rate in the dc limit. An increase in laser intensity from 1.0×10^{14} to 2.0×10^{14} W cm^{-2} results in a similar outer peak with an about seven-fold increase in the ionization rate.

(Some figures may appear in colour only in the online journal)

1. Introduction

The study of ionization of atoms and molecules by continuous-wave (CW) strong-field lasers in the optical and infrared regimes has evolved to a good level of understanding. Dissociative ionization of small molecules was reviewed in [1]. Experimentally, the focus has shifted towards short pulses, since pulse compression allows for stronger fields, but studies of the hydrogen molecular ion in intense laser fields were also carried out in the CW regime [2], particularly for infrared light [3]. Theoretically, the CW case can be treated by standard Floquet theory, while short pulses are dealt with by solving the time-dependent Schrödinger equation directly [4]. In addition, multi-mode Floquet analysis allows a pulse envelope to be taken into account [5]. While much focus has shifted towards understanding detailed phenomena, such as electron spectra and high harmonic generation from many-electron molecules [6], there is still some need to explore ionization rates as a function of internuclear separation R for the simplest molecule, namely the hydrogen molecular ion H_2^+.

The interest in the R-dependent ionization rates for the lowest molecular eigenstates arises for several reasons: in laser-pulse experiments the neutral molecule is often ionized by the rising pulse and produces a molecular ion in a dissociating state, i.e., a high vibrational mode of the molecule is excited [7, 8]. The strong field may also mix the lowest two electronic eigenstates. As the molecule expands the ionization rates for both states increase substantially, and the laser may ionize the molecule efficiently at so-called critical separations R_c [3]. Vibrational population trapping is also predicted [9]. It is possible to determine the actual distance R when ionization

Table 1. The Keldysh parameter values for the $1s\sigma_g$ and $2p\sigma_u$ states of the H_2^+ ion at various separations R (in au), and laser intensity $I = 10^{14}$ W cm^{-2}.

States	λ (nm)	ω	$R = 2$	$R = 4$	$R = 6$	$R = 8$	$R = 10$	$R = 12$
$1s\sigma_g$	1064	0.0428	1.18	1.01	0.93	0.89	0.88	0.87
	2280	0.02	0.56	0.47	0.44	0.42	0.41	0.40
	4560	0.01	0.28	0.24	0.22	0.21	0.21	0.20
$2p\sigma_u$	1064	0.0428	0.93	0.95	0.92	0.90	0.88	0.87
	2280	0.02	0.43	0.44	0.43	0.42	0.41	0.40
	4560	0.01	0.22	0.22	0.21	0.21	0.21	0.20

occurred from a measurement of the kinetic energies of the molecular fragments.

Experiments were thus able to confirm at least parts of the pattern of the ionization rate versus R obtained from theoretical calculations. However, the structures in the ionization rate predicted for larger internuclear separations R could not be found in some experiments [4]. Other experiments with carefully prepared H_2^+ ions with short (100 fs) laser pulses and a wavelength of 791 nm were able to find evidence of three larger-R maxima in the ionization rate [10, 11].

Structures in the R-dependent ionization rate were found theoretically in the dc limit [12–15] for the upper state. The physical mechanism for strong-field ionization in this limit is tunnelling for the lower state, and small-barrier tunnelling or over-the-barrier escape for the upper state depending on the field strength and separation R. The calculations are deemed mature, with different methods confirming earlier results, and resulting in a high degree of precision in the resonance positions and widths for the single-electron molecule. Interestingly, the peaking structures in the ionization rate for the upper state are quite similar to those of ac Stark calculations. It is therefore deemed interesting to search for a connection, and particularly to explore the small-ω limit of the ac case.

In atomic photoionization one can distinguish between the tunnelling and multi-photon ionization regimes with the help of the Keldysh parameter, defined as $\gamma = \sqrt{|E_b|/2U_p}$ where E_b is the electron binding energy and $U_p = (F/2\omega)^2$ is the pondermotive energy with F the laser electric field strength and ω the angular frequency in atomic units. A value of $\gamma \ll 1$ corresponds to tunnelling ionization, $\gamma \sim 1$ indicates the intermediate regime, and $\gamma \gg 1$ multi-photon ionization. In table 1 we show the Keldysh parameter values for chosen wavelength λ values and a field intensity of $I = 10^{14}$ W cm^{-2}, for the ground and first excited states of the H_2^+ ion. It is known, however, that in the molecular case matters are more complicated, especially at intermediate internuclear separations R [16]. The complicated behaviour was associated with non-adiabatic electron localization near the nuclei.

The Floquet analysis of the strong-field ac Stark problem was pioneered for atomic hydrogen by Shakeshaft and co-workers [17]. For the hydrogen molecular ion the R-dependent peak structures were analysed by Madsen and Plummer [18] with ideas based on Floquet channel couplings to identify which mechanism was responsible for them: as an alternative to tunneling they offered explanations in terms of resonance-enhanced multi-photon ionization (REMPI). In a naive, intuitive picture one might think that in the presence of a tunnelling barrier the small-ω limit implies that ionization is effective only during the peak of the field: during a cycle this will occur twice (once to each side), and re-scattering of electrons ionized during earlier cycles will also take place. The Floquet picture, on the other hand, suggests that photo-ionization in a small-ω CW laser field is a complicated process, requiring the coupling of very many channels to make an accurate prediction. It also suggests that the lower and upper states become highly mixed. It appears then that the Keldysh parameter values which decrease with ω are perhaps misleading in the molecular case. This is obviously the case for the upper state which is not affected by an outer potential barrier at intermediate and large R. As will be shown below, the lower state is mixing with the upper state in this R-regime, and, thus, the Keldysh argument has to be used carefully in the molecular intermediate-R case.

The purpose of this paper is to illustrate the Floquet results systematically in the limit of small laser frequency. Using a methodology similar to previous work at λ = 1064 nm, we confirm a number of prior results and also find some small discrepancies. New features are found as the IR wavelength is pushed further into the μm regime.

2. Theory

2.1. The Floquet Hamiltonian

We treat the hydrogen molecular ion, H_2^+ in the Born–Oppenheimer approximation, in which the two nuclei are fixed, and only the electronic motion is taken into account. The field-free electronic Hamiltonian of the H_2^+ molecule can be written in atomic units as

$$H_0 = -\frac{1}{2}\nabla_{\mathbf{r}}^2 - \frac{1}{\left|\mathbf{r} + \frac{R}{2}\mathbf{e}_z\right|} - \frac{1}{\left|\mathbf{r} - \frac{R}{2}\mathbf{e}_z\right|}, \tag{1}$$

where $\mathbf{r}$ is the electron position vector and R is the internuclear separation.

If we assume that the interaction of the electron with the external electric field $V_L(\mathbf{r}, t)$ is periodic in time with period $T = 2\pi/\omega$, that is, $H(\mathbf{r}, t+T) = H(\mathbf{r}, t)$, according to Floquet theory [19, 20], the solution $\Psi(\mathbf{r}, t)$ to the time-dependent Schrödinger equation for the system

$$\mathrm{i}\frac{\partial}{\partial t}\Psi(\mathbf{r}, t) = H(t)\Psi(\mathbf{r}, t) = [H_0 + V_L(\mathbf{r}, t)]\Psi(\mathbf{r}, t), \tag{2}$$

can be written as

$$\Psi(\mathbf{r}, t) = \mathrm{e}^{(-\mathrm{i}E_F t)}\Phi(\mathbf{r}, t), \tag{3}$$

$$\Phi(\mathbf{r}, t + T) = \Phi(\mathbf{r}, t) = \sum_{n=-\infty}^{\infty} \mathrm{e}^{\mathrm{i}n\omega t}\phi_n(\mathbf{r}), \tag{4}$$

where E_F is called the Floquet quasi-energy, and the $\phi_n(\mathbf{r})$ obey time-independent coupled-channel equations.

Substitution of the solution (3) into the Schrödinger equation (2) leads to a time-dependent eigenvalue problem:

$$H_F(\mathbf{r},t)\Phi(\mathbf{r},t) = E_F\Phi(\mathbf{r},t), \tag{5}$$

where the Floquet Hamiltonian $H_F(\mathbf{r},t)$ is defined as

$$H_F(\mathbf{r},t) = H(\mathbf{r},t) - \mathrm{i}\frac{\partial}{\partial t}. \tag{6}$$

In this work we assume that the external field is provided by a linearly polarized monochromatic laser aligned with the internuclear axis of the H_2^+ ion, and that the dipole approximation is valid. Then the interaction $V_L(\mathbf{r},t)$ takes the form

$$V_L^{\mathrm{lg}}(\mathbf{r},t) = Fz\cos\omega t, \tag{7}$$

in length gauge, and

$$V_L^{\mathrm{vg}}(\mathbf{r},t) = \mathrm{i}\frac{F}{\omega}\sin\omega t\frac{\partial}{\partial z} + \frac{F^2}{2\omega^2}\sin^2\omega t \tag{8}$$

in velocity gauge, where F is the laser field strength. The length gauge is more appropriate for low-frequency fields, while the velocity gauge is valuable for intermediate-frequency laser fields. We employ both gauges for $\omega = 0.0428$ au, and the length gauge alone for smaller values of ω.

For the solution of the Floquet (*steady-state*) Hamiltonian (6), the time variable t is treated in analogy to a coordinate variable, and the Schrödinger equation (5) is solved as for the stationary states of the time-independent Schrödinger equation. Once we find $\Phi(\mathbf{r},t)$ from the *steady-state* Schrödinger equation (5), we obtain the solution $\Psi(\mathbf{r},t)$ to the time-dependent Schrödinger equation (2) via equation (3).

We choose prolate spheroidal coordinates to deal with the H_2^+ ion, in which the Born–Oppenheimer treatment (equation (1)) gives an analytic solution to the Schrödinger equation [21–23]. We transform $\mathbf{r}$ to prolate spheroidal coordinates μ, ν, and φ, which are related to the Cartesian coordinates x, y and z as follows:

$$x = \frac{R}{2}\sqrt{(\mu^2-1)(1-\nu^2)}\cos\varphi, \tag{9}$$

$$y = \frac{R}{2}\sqrt{(\mu^2-1)(1-\nu^2)}\sin\varphi, \tag{10}$$

$$z = \frac{R}{2}\mu\nu, \quad 1 \leqslant \mu < \infty, \quad -1 \leqslant \nu \leqslant 1, \quad 0 \leqslant \varphi \leqslant 2\pi. \tag{11}$$

The field-free Hamiltonian (1) and $\partial/\partial z$ are given as

$$H_0 = -\frac{1}{2}\frac{4}{R^2(\mu^2-\nu^2)}\left[\frac{\partial}{\partial\mu}\left[(\mu^2-1)\frac{\partial}{\partial\mu}\right] + \frac{\partial}{\partial\nu}\left[(1-\nu^2)\frac{\partial}{\partial\nu}\right] + \frac{\mu^2-\nu^2}{(\mu^2-1)(1-\nu^2)}\frac{\partial^2}{\partial\varphi^2}\right] - \frac{4\mu}{R(\mu^2-\nu^2)}, \tag{12}$$

$$\frac{\partial}{\partial z} = \frac{2}{R(\mu^2-\nu^2)}\left[\nu(\mu^2-1)\frac{\partial}{\partial\mu} + \mu(1-\nu^2)\frac{\partial}{\partial\nu}\right]. \tag{13}$$

Here we limit ourselves to Σ electronic states (no φ dependence).

Since the solution to the Schrödinger equation with Hamiltonian (12) is found analytically in terms of Legendre polynomials, it is natural to employ a Legendre-based pseudospectral method [24, 25]. We do not discuss the details of this methodology here, they can be found in [15]. It is similar to that of [14], except that we do not symmetrize the Hamiltonian, which yields improved computational efficiency. We arrived at this conclusion by comparing the convergence properties of bound-state pseudospectral representations given in [26]. Photoionization of H_2^+ by short UV laser pulses has been treated recently by analogous grid methods for the *time-dependent* Schrödinger equation [27–30].

2.2. AC Stark-resonance Hamiltonian and the complex absorbing potential method

The ac Stark resonance Hamiltonian in prolate spheroidal coordinates is given as

$$H_{\mathrm{res}}(\mu,\nu,t) = H_0(\mu,\nu) + V(\mu,\nu,t). \tag{14}$$

To avoid the calculation of outgoing waves we add an artificial complex absorbing potential (CAP) to this Hamiltonian. One needs to choose this CAP only for the coordinate μ:

$$H = H_{\mathrm{res}}(\mu,\nu,t) - \mathrm{i}\eta W(\mu),$$
$$W(\mu) = \Theta(\mu-\mu_c)(\mu-\mu_c)^2, \tag{15}$$

where Θ is the Heaviside step function, η is a small positive parameter, and μ_c determines the ellipse outside of which the CAP dampens the outgoing wave in the asymptotic region. This means that the eigenfunction of the resonance state can be solved for in a square-integrable basis, that is, one solves an eigenvalue problem to find complex energy eigenvalues, whose real part yields the resonance position, and the inverse of the imaginary part is associated with the lifetime of that state.

While using a finite basis set, ideally we want η to be small to produce a small artefact. However, when the parameter η tends to zero, the computational representation error increases. Thus, we want η to not be too small to have an easier (or more accurate) calculation. Then, we remove the artefact due to the CAP. This can be done by the iterative correction method of Riss and Meyer [31], or by a Padé extrapolation method [32–34]. Following [31] we have

$$E^{(n)} = E^{(n)}(\tilde{\eta}) = E_{\mathrm{fb}}(\tilde{\eta}) + \sum_{j=1}^{n}\frac{(-\tilde{\eta})^j}{j!}\left.\frac{\mathrm{d}^j E_{\mathrm{fb}}}{\mathrm{d}\eta^j}\right|_{\eta=\tilde{\eta}}, \tag{16}$$

where $\tilde{\eta}$ is an optimal value found by the condition [31]

$$\left|\frac{\eta^{n+1}}{(n+1)!}\left.\frac{\mathrm{d}^{n+1}E_{\mathrm{fb}}}{\mathrm{d}\eta^{n+1}}\right|_{\eta=\tilde{\eta}}\right| = \min,\ n = 0, 1, 2, 3. \tag{17}$$

Here E_{fb} stands for finite-basis eigenvalues calculated on an η-grid.

Following equation (5) in [34], (cf [32]) a Padé approximant for $E_{\mathrm{fb}}(\tilde{\eta})$ is obtained from

$$E_{\mathrm{Padé}}(\eta) = \frac{\sum_{i=0}^{N_1} p_i\eta^i}{1+\sum_{j=1}^{N_1+1} q_j\eta^j}, \tag{18}$$

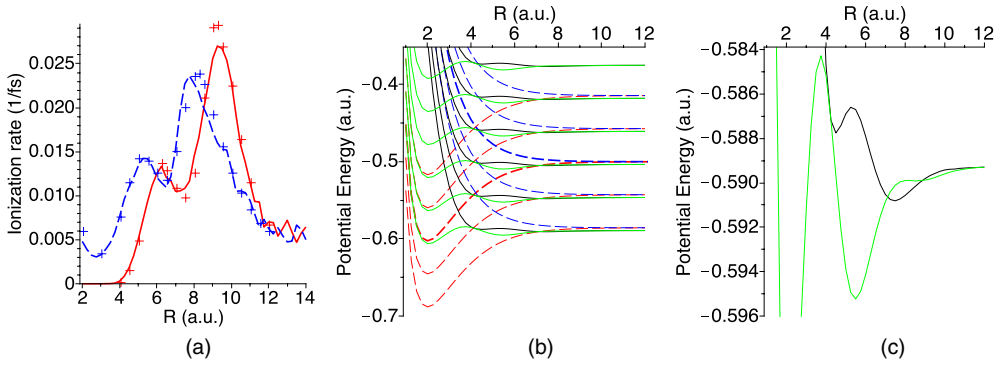

Figure 1. (a) The ionization rates (in fs^{-1}) as a function of R for the lower and upper states of H_2^+. Curves: present results, solid red for the lower state, and dashed blue for the upper state; crosses: Chu *et al* [14]: (b) for the lower and upper states of the ion, the field-dressed diabatic potential red (lower) and blue (upper) curves are dashed, respectively, and the corresponding adiabatic potential curves are presented by solid green (lower) and black (upper) curves. (c) The magnified detail of (b), showing clearly true and avoided crossings for the adiabatic potential curves. The field parameters are $F = 0.0533$ au and $\omega = 0.0428$ au.

where p_i and q_j are complex coefficients, and $N_p = 2(N_1 + 1)$ is the number of points used in the approximant. We found that $N_p = 4$ yielded reasonable extrapolations to $\eta = 0$. In the present work we found that the Riss–Meyer method with order $n = 2$ and the extrapolation method gave very consistent results.

With the complex Hamiltonian equation(15), the time-independent coupled equations are

$$[H_0(\mu, \nu) - i\eta W(\mu)]\phi_n(\mu, \nu) + \tfrac{1}{2}Fz[\phi_{n-1} + \phi_{n+1}] = (E_F - n\omega)\phi_n(\mu, \nu), \quad (n = 0, \pm1, \pm2 \ldots) \tag{19}$$

in length gauge, and

$$[H_0(\mu, \nu) - i\eta W(\mu)]\phi_n(\mu, \nu) + \frac{1}{2}\frac{F}{\omega}\frac{\partial}{\partial z}[\phi_{n-1} - \phi_{n+1}] = (E_F - n\omega)\phi_n(\mu, \nu), \quad (n = 0, \pm1, \pm2 \ldots) \tag{20}$$

in velocity gauge, and are discretized as shown in [15]. In (20) we removed the overall phase proportional to F^2, as it does not affect the results.

3. Results and discussion

In figure 1 we show results for the previously studied case of $\lambda = 1024$ nm where the Keldysh parameter is of order unity (the intensity of the laser field equals 10^{14} W cm^{-2}). The ionization rates as a function of separation R (obtained as $-2\Im(E_F)$) are shown in panel (a) for the lower and upper states starting with the equilibrium values ($R = 2$ au) for the upper state. The lower state has a very small ionization rate for $R < 4$ au due to the large outer tunnelling barrier. The upper-state ionization rate displays an undulating pattern with distinct peaks at $R = 5.5$ au and $R = 7.75$ au. The lower-state ionization rate rises to match the upper-state rate between the peaks, and then surpasses the upper-state rate (peak at $R = 9.5$ au).

Our results are in reasonable agreement with those of Chu and Chu [14] with some notable differences in the region beyond the first peaks. We carried out a substantial convergence analysis to confirm our results in both the length and velocity gauges. The convergence properties of the Floquet calculations in velocity versus length gauge can be characterized as follows. For larger ω than of interest in this work, such as $\omega = 0.2$ au at the equilibrium proton separation of $R = 2$ au we found convergence in resonance position and width for the upper state to be better than 7 digits for 21 channels in velocity gauge, and 25 channels in length gauge. At a wavelength of $\lambda = 1024$ nm, or $\omega = 0.0428$ au 57 channels were required in length gauge to achieve this accuracy, while a 65-channel calculation in velocity gauge only resulted in absolute 5-digit accuracy. For $\omega = 0.02$ au the length gauge calculation was 7-digits accurate at 49 channels, while the velocity gauge yielded poor results even at 65 coupled channels. Therefore, the length gauge was deemed most appropriate for the present low-ω work.

In figure 1(b) we show the Floquet potential energy curves. One can understand the mixing of the lower and upper states for $R > 4$ au on the basis of this diagram. The field-dressed diabatic potential curves for the lower and upper states are shown by dashed red (lower) and dashed blue (upper) curves, which are obtained from equations (19) or (20) in the absence of an external field, i.e., for $F = 0$. The non-diagonal coupling term caused by the external field vanishes in this limit, and the eigenvalues of the *Hermitian* Hamiltonian yield the diabatic curves. These diabatic curve pairs are shifted from each other by $\pm n\omega$, where n is the number of photons absorbed or emitted [18]. The bold dashed red and blue curves represent the zero-photon lower ($1s\sigma_g - 0\omega$) and upper ($2p\sigma_u - 0\omega$) states. While the lowest diabatic curve for the lower state shown in (b) corresponds to the $1s\sigma_g - 2\omega$ state, the highest diabatic curve for the upper state represents the $2p\sigma_u + 2\omega$ state. The lower/upper state curves for different values of n undergo true crossings. The corresponding adiabatic potential curves for the lower and upper states are represented by solid green (lower) and solid black (upper) curves, which are obtained in presence of the external field, that is, from the full non-Hermitian resonance Floquet Hamiltonian calculation (19) or (20). The adiabatic curves undergo avoided crossings where true crossings occur in the diabatic levels.

In panel (c) of figure 1 the potential energy curves for the $n = 0$ Floquet channel are shown on a fine scale. Following the methodology of Madsen and Plummer [18] (based on [17]) we

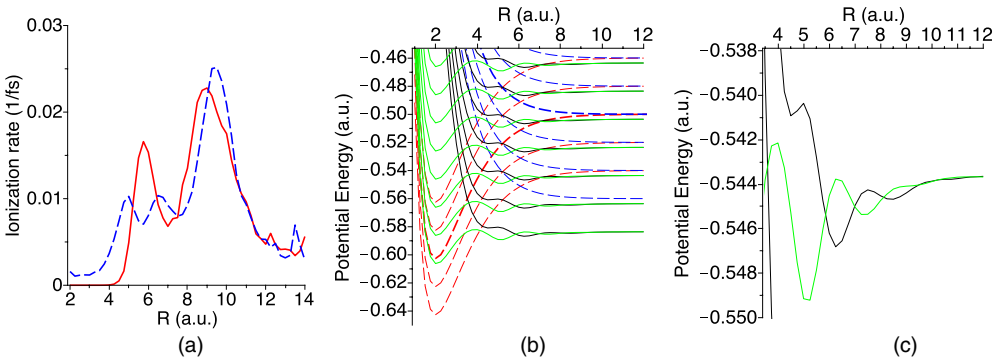

Figure 2. The same as in figure 1, but $F = 0.0533$ au and $\omega = 0.02$ au.

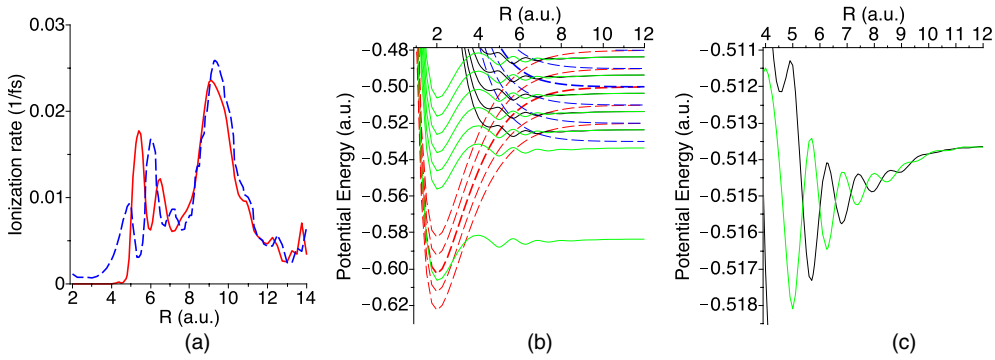

Figure 3. The same as in figure 1, but $F = 0.0533$ au and $\omega = 0.01$ au.

tracked carefully the real and imaginary parts of the Floquet eigenvalues as a function of R. The complex energies are not allowed to cross (the Hamiltonian depends adiabatically on R). The crossing is avoided either in the real or in the imaginary part. A true crossing in the real part of the complex energy is associated with an avoidance structure in the imaginary part, i.e., the ionization rate acquires complicated behaviour with maxima and minima as a function of R.

In figures 2 and 3 we proceed with the same strategy to understand the behaviour as the laser wavelength is moved further into the infrared regime. The following picture emerges: starting with $R > 4$ au the ionization rates for the two states intertwine; in the first peak region ($R \approx 5.5$ au) this intertwining phenomenon is oscillatory with the number of oscillations increasing with decreasing ω. In the second peak region ($R \approx 9.5$ au), the ionization rates for the upper and lower states track each other with apparently a better match as ω is lowered.

Panels (b) and (c) of figures 2 and 3 show the systematic reasons for the observed behaviour. On the energy scale set by the two molecular eigenstates as a function of R the number of participating Floquet channels increases as ω is reduced (in inverse proportion). While the figures show only a limited number of Floquet channels, converged resonance parameter values were calculated on the basis of at least 64 ($\omega = 0.0428$ au), 80 ($\omega = 0.02$ au) and 100 ($\omega = 0.01$ au) channel calculations.

We have carried out calculations for smaller ω (further reduced by a factor of 2 and 4) with the finding that the number of oscillations in the region of the first peak keeps increasing. These calculations are more time-consuming, as the number of Floquet channels to be coupled increases correspondingly.

From the comparison of the ionization rates shown in figures 1–3(a) we can make an interesting observation: the scale of the ionization rate appears to be quite independent of ω. We note that the widths of the Floquet resonances are still quite reasonable (below 10^{-3} au). A physical reason for the independence of the ionization rate on the laser frequency ω can be given on the basis of the ionization mechanism. In the strong-field regime ionization can be understood via tunnelling or an over-barrier mechanism as occurring for certain periods of time during the laser cycle (when the field is close to its peak value). Strong ω dependence can be expected in a multi-photon regime. From the present work it becomes clear that electron localization in one of the two wells is happening near the critical radii, and this is determining the upper- and lower-state ionization rates. The ω parameter plays an important role in the technical aspects of the calculation only, since it controls the number of Floquet channels that participate.

In [15] it was shown for the dc Stark problem how the peak structures in the ionization rates were associated with changes in the pattern of the localized probability density of the decaying Siegert states. For the present ac case, an analogous presentation is more complicated due to the time-dependence (during one period of the laser field $T = 2\pi/\omega$). With a certain caveat, we provide such a presentation in figures 4 and 5 for the case of $\omega = 0.01$ au in order to illustrate the oscillatory pattern in the ionization rate. We chose two separations: in

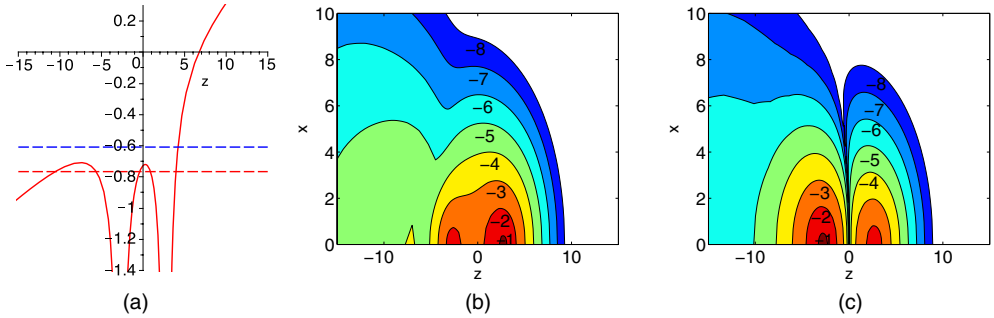

Figure 4. (a) Electronic potential and real parts of electronic quasienergies for the lower and upper states (reference channel $n = 0$) and (b), (c) contour plots of $\log|\Phi(\mathbf{r}, t = 0, T)|^2$ for the lower, and upper states for H_2^+ at $R = 5.5$ au, and $F = 0.0533$ au and $\omega = 0.01$ au. Note that the x-axis is scaled differently from the z-axis, i.e., the outflow is mostly along the direction of the laser field. The x- and z-axis are labelled in *au*.

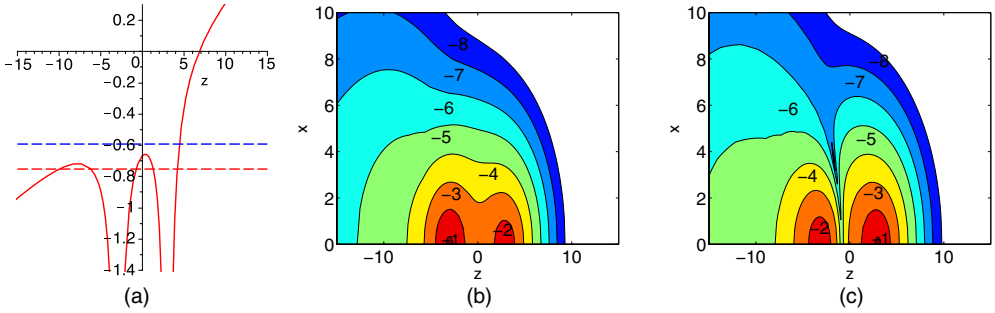

Figure 5. The same as in figure 4, but at $R = 6$ au, and $F = 0.0533$ au and $\omega = 0.01$ au.

figure 4 for $R = 5.5$ au the lower state has a local maximum, while the upper state has a minimum in the ionization rate; in figure 5 for $R = 6$ au the situation is reversed.

The plots represent the time when the field is at its peak, i.e., they represent a snapshot of the density which has moved to the left with the laser field. For the range of small ω values used in this work these (left–right) oscillations track the field reasonably well.

Panels (a) of figures 4 and 5 show cuts through the potential along the molecular axis (at $t = 0, T$), as well as the resonance positions for both states (which are averaged over one cycle). They show the lower state as trapped (internal and external barrier), and the upper state as untrapped for both separations.

A comparison of the densities for the lower state shows that at $R = 5.5$ au (figure 4(b)) the state is more concentrated in the right well, and therefore ionizes rather easily. At $R = 6$ au (figure 4(b)), on the other hand, the lower state displays more localization in the left well, resulting in a reduced ionization rate. This shows that the simple diagram (4(a)) is insufficient to explain the ionization rate behaviour: the fact that the lower state localizes in the right-hand well for $R = 5.5$ au gives it apparently the 'over-the-inner-barrier' higher ionization property rather than tunnelling behaviour. This localization (or state-mixing) issue is the main reason why one has to be careful in applying the Keldysh parameter argument, which usually works well for atoms and equilibrium-R molecules. In the language of Floquet theory, this state mixing is referred to as REMPI [18].

The upper-state densities (figures 4(c) and 5(c) show a reversed behaviour. The lower- and upper-state densities are distinct from each other: one can clearly see the remnants of a nodal structure of the field-free upper state (low-density region to the left of $z = 0$), while the lower state resembles the symmetry character of the field-free state in the internuclear region.

Therefore, one can argue on the basis of the density plots that Floquet channel couplings occur in such a way that in the region of the first peak in the ionization rate the states maintain some of their identity even though their complex energies become intertwined. As one varies the separation R the lower-state density has maxima at either nucleus that vary dramatically in height. This causes the ionization rate to be strongly modulated as R is varied. The upper state has a complementary oscillation pattern. These density plots may very well give support to the ideas of adiabatic electronic localization raised in [16].

For large R, when there is an inner tunnelling barrier, the density localized near the nuclei oscillates with period $T = 2\pi/\omega$. For small ω it can, in fact, oscillate out of phase with the external field. While the individual stationary Floquet channel functions $\phi_n(\mathbf{r})$ are either symmetric or anti-symmetric, their superposition with complex amplitudes $e^{in\omega t}$ can display tunnelling oscillations with period T.

Finally, we show in figure 6 also a density plot for the larger-R peak region, namely near the maximum in the ionization rate ($R = 9.25$ au). The energy levels superimposed on a snapshot of the potential along the molecular axis show that both states are energetically above the outer barrier on this

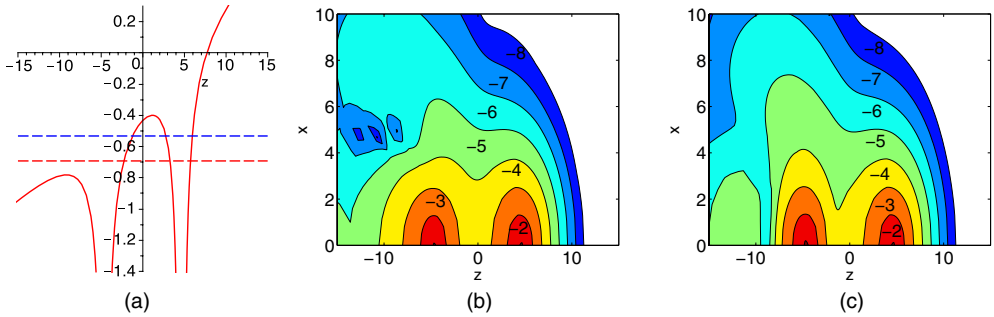

Figure 6. The same as in figure 4, but at $R = 9.25$ au, and $F = 0.0533$ au and $\omega = 0.01$ au.

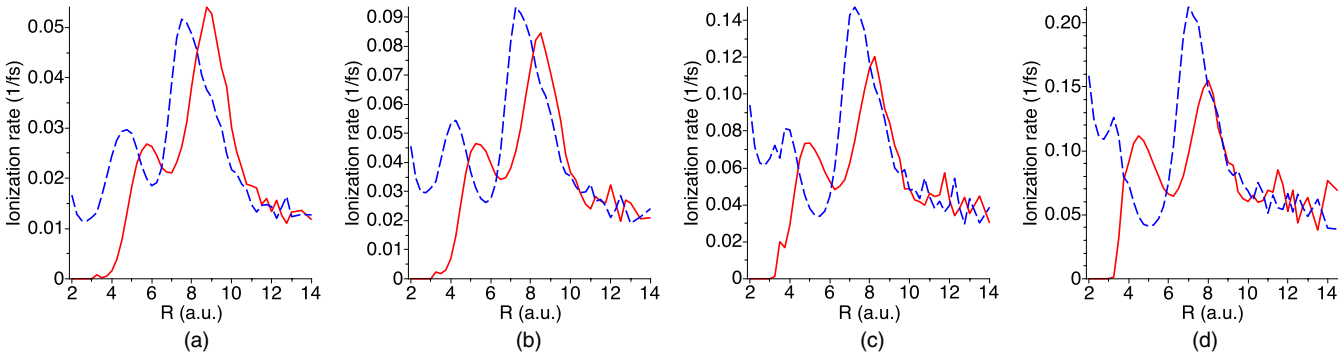

Figure 7. The ionization rates (in fs^{-1}) as a function of R for the lower and upper states of H_2^+. Curves: present results, solid red for the lower state, and dashed blue for the upper state. (a) $I = 1.25 \times 10^{14}\,\mathrm{W\,cm^{-2}}$: (b) $I = 1.5 \times 10^{14}\,\mathrm{W\,cm^{-2}}$: (c) $I = 1.75 \times 10^{14}\,\mathrm{W\,cm^{-2}}$: (d) $I = 2.0 \times 10^{14}\,\mathrm{W\,cm^{-2}}$, and $\omega = 0.0428$ au.

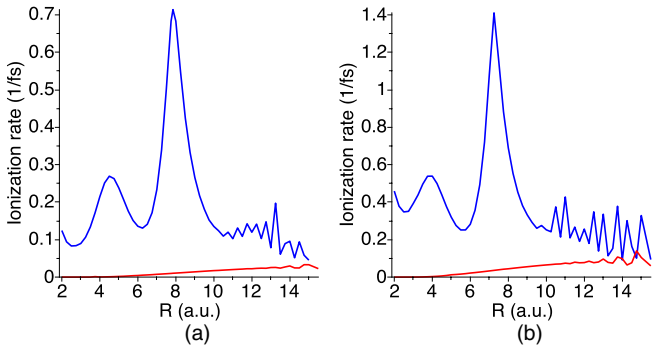

Figure 8. The dc-limit ionization rates (in fs^{-1}) as functions of internuclear separation R for the lower (red) and upper (blue) states of H_2^+. The dc field intensities are $I = 1.5 \times 10^{14}$ W cm^{-2} (a) and $I = 2.0 \times 10^{14}$ W cm^{-2} (b). The corresponding results for $I = 1.0 \times 10^{14}$ W cm^{-2} are shown in [15].

case, but that there is an inner barrier to overcome. Both states have similar density patterns, i.e., the upper state has lost its nodal structure completely (as was observed for the dc case in [15]). Thus, we can assume that complete state-mixing occurs in the region of the larger-R peak. Eventually, with increasing R the inner barrier rises, and ionization becomes less effective.

In figure 7 we present some additional results to show how the ionization rates change with laser intensity. It can be seen that the only moderately stronger fields result in some changes in the ionization patterns for small and intermediate R values. While the lower state for $R \ll 4$ au is still governed by tunnelling ionization, the regime where it mixes with the upper state begins at $R \approx 4$ au for the doubled intensity. The ionization rate for the upper state increases dramatically even at the equilibrium separation. For the outer critical radii we notice that they are also somewhat reduced with the lower state experiencing a less dramatic increase in ionization rate. When we average the outer peaks for the two states we find approximately a seven-fold increase in ionization rate with doubled intensity. The intermediate cases (panels (b), (c)) indicate that the changes occur gradually.

In order to test our conclusions about the relation of the results to the dc limit findings for the upper state we show the dc limit results for two laser intensities in figure 8. These results (which are much easier to obtain technically, as there is no channel convergence to worry about and the analysis of the complex eigenvalue spectrum is straightforward) also show similar features as the field intensity increases: at the outer critical radius ($R_c \leqslant 8$ au) we find an approximately seven-fold increase in ionization rate (for the upper state), the peak structure narrows and moves slightly towards smaller R. For $R > 12$ au the ionization rates for the upper and lower states become competitive. In the large-R limit the rates coalesce, since the two complex eigenvalues become nearly degenerate. In figure 9 the ionization rates as a function of internuclear separation R are shown for two laser frequencies at a field intensity of $I = 2.0 \times 10^{14}$ W cm^{-2}. The results for the lower and upper states merge for large R as $\omega \to 0$. They do resemble the dc limit for the upper state near $R = 8$ au with the ac rate for both states approaching 15% of the dc upper-state value.

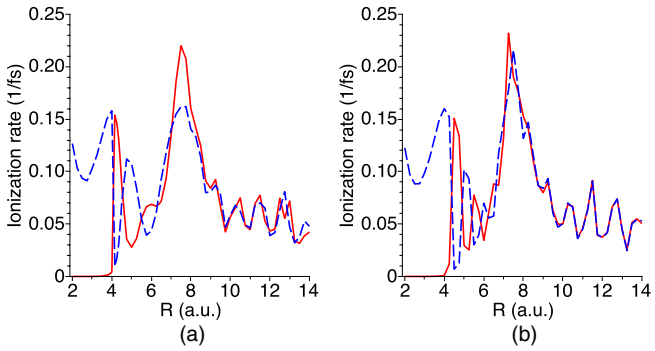

Figure 9. The same as in figure 7, but the field parameters are $\omega = 0.02$ au (a) $\omega = 0.01$ au (b) and $I = 2.0 \times 10^{14}$ W cm^{-2}.

4. Conclusions

Floquet calculations in a pseudospectral representation for the lowest two H_2^+ eigenstates are shown to display rather different behaviour in the small-ω limit for the two peak regions in the ionization rate.

For the first peak region ($R \approx 5$ au) the density plots of the coupled-channel Floquet eigenfunctions demonstrate that while the upper state has remnants of a nodal structure (near $z = 0$), the ionization rates oscillate against each other as a function of R. The oscillation pattern becomes more rapid as $\omega \to 0$.

The outer peak region ($R \approx 9$ au) shows a different situation. The upper- and lower-state density plots have similar structures in between the nuclei. The inner tunnelling barrier causes localized density to oscillate from one nucleus to the other as a function of time. The ionization rates for the upper and lower states become the same in this region.

Finally, we note that for the large-R peak the calculated ionization rates seem to approach an $\omega \to 0$ limit. The rates are approximately 10–15% of those found in the dc limit for the upper state [15]. This should be considered reasonable, since in the ac case the field is at a strength close to its peak value for about one tenth of the laser cycle.

We tested our findings in a limited range of intensities for which the lower state at equilibrium separation $R = 2$ au has a small ionization rate due to the large tunnelling barrier. The upper state, however, ionizes quite readily even for $R = 2$ au via an over-the-barrier mechanism. Since lasers of higher intensities are becoming available, it will be of interest to extend these calculations to stronger fields to explore the regime where the lower state will also experience strong ionization at small R.

Acknowledgments

We thank the Natural Sciences and Engineering Research Council of Canada for financial support, and the Shared Hierarchical Academic Research Computing Network [35] for access to high-performance computing facilities.

References

[1] Codling K and Frasinski L J 1993 *J. Phys. B: At. Mol. Opt. Phys.* **26** 783
[2] Giusti-Suzor A *et al* 1995 *J. Phys. B: At. Mol. Opt. Phys.* **28** 309
[3] Walsh T D G, Strach L and Chin S L 1998 *J. Phys. B: At. Mol. Opt. Phys.* **31** 4853
[4] Ben-Itzhak I *et al* 2008 *Phys. Rev.* A **78** 063419
[5] Huang Y and Chu S-I 1994 *Chem. Phys. Lett.* **225** 46
[6] Smirnova O *et al* 2009 *Nature* **460** 972
[7] Ivanov M, Seideman T, Corkum P, Ilkov F and Dietrich P 1995 *Phys. Rev.* A **54** 1541
[8] Chelkowski S and Bandrauk A D 1995 *J. Phys. B: At. Mol. Opt. Phys.* **28** L723
[9] Giusti-Suzor A and Mies F H 1992 *Phys. Rev. Lett.* **68** 3869
[10] Trump C *et al* 2008 *Phys. Rev.* A **62** 063402
[11] Pavičić D, Kiess A, Hänsch T W and Figger H 2005 *Phys. Rev. Lett.* **94** 163002
[12] Plummer M and McCann J F 1996 *J. Phys. B: At. Mol. Opt. Phys.* **29** 4625
[13] Mulyukov Z, Pont M and Shakeshaft R 1996 *Phys. Rev.* A **54** 4299
[14] Chu Xi and Chu S-I 2000 *Phys. Rev.* A **63** 013414
[15] Tsogbayar Ts and Horbatsch M 2013 *J. Phys. B: At. Mol. Opt. Phys.* **46** 085004
[16] Seideman T, Ivanov M Yu and Corkum P B 1995 *Phys. Rev. Lett.* **75** 2819
[17] Shakeshaft R and Potvliege R M 1987 *Phys. Rev.* A **36** 5478
[18] Madsen L B and Plummer M 1998 *J. Phys. B: At. Mol. Opt. Phys.* **31** 87
[19] Floquet G 1883 *Ann. Ec. Norm. Suppl.* **12** 47
[20] Sambe H 1973 *Phys. Rev.* A **7** 2203
[21] Hylleraas E A 1931 *Z. Phys.* **71** 739
[22] Jaffé G 1934 *Z. Phys.* **87** 535
[23] Baber W G and Hassé H R 1935 *Proc. Camb. Phil. Soc.* **31** 564
[24] Funaro D 1992 *Polynomial Approximation of Differential Equations* (Berlin: Springer)
[25] Hesthaven J S, Gottlieb S and Gottlieb D 2007 *Spectral Methods for Time-Dependent Problems* (Cambridge: Cambridge University Press)
[26] Kokoouline V, Dulieu O, Kosloff R and Masnou-Seeuws F 1999 *J. Chem. Phys.* **110** 9865
[27] Telnov D A and Chu S-I 2005 *Phys. Rev.* A **71** 013408
[28] Tao L, McCurd C W and Rescigno T N 2009 *Phys. Rev.* A **80** 013402
[29] Guan X, Secor E B, Bartschat K and Schneider B I 2011 *Phys. Rev.* A **84** 033420
[30] Guan X, DuToit R C and Bartschat K 2013 *Phys. Rev.* A **87** 053410
[31] Riss U V and Meyer H-D 1993 *J. Phys. B: At. Mol. Opt. Phys.* **26** 4503
[32] Lefebvre R, Sindelka M and Moiseyev N 2005 *Phys. Rev.* A **72** 052704
[33] Santra R 2006 *Phys. Rev.* A **74** 034701
[34] Ackad E and Horbatsch M 2007 *Phys. Rev.* A **76** 022503
[35] SHARCNET: Shared Hierarchical Academic Research Computing Network (www.sharcnet.ca)